

**TITLE**

Evidence for the Key Role of H<sub>3</sub>O<sup>+</sup> in Phospholipid Membrane Morphology

Charles G. Cranfield<sup>1\*</sup>, Thomas Berry<sup>1</sup>, Stephen A. Holt<sup>2</sup>, Khondker R. Hossain<sup>1,2</sup>, Anton P. Le Brun<sup>2</sup>, Sonia Carne<sup>3</sup>, Heba Al Khamici<sup>1</sup>, Hans Coster<sup>4</sup>, Stella M. Valenzuela<sup>1</sup> and Bruce Cornell<sup>3</sup>

**AUTHOR AFFILIATIONS**

<sup>1</sup>School of Life Sciences, University of Technology Sydney, Ultimo, NSW 2007, Australia.

<sup>2</sup>Australian Nuclear Science and Technology Organisation, Locked Bag 2001 Kirrawee DC, New South Wales 2232, Australia. <sup>3</sup>SDx Tethered Membranes Pty Ltd, Unit 6 30-32 Barcoo St, Roseville NSW 2069, Australia. <sup>4</sup>School of Chemical and Biomolecular Engineering, University of Sydney, NSW 2006, Australia.

**CORRESPONDING AUTHOR**

\*Charles Cranfield, School of Life Sciences, University of Technology Sydney, Ultimo, NSW 2007, Australia. Ph +61 9514 4034. E-mail: [charles.cranfield@uts.edu.au](mailto:charles.cranfield@uts.edu.au)

**KEYWORDS**

Tethered bilayer lipid membranes (tBLMs), hydrogen bond, pH regulation, impedance spectroscopy, neutron reflectometry.

## ABSTRACT

This study identifies the importance of the phosphate moiety and  $\text{H}_3\text{O}^+$  in controlling the ionic flux through phospholipid membranes. We show that despite increasing the  $\text{H}_3\text{O}^+$  concentration when lowering the pH, the ionic conduction through phospholipid bilayers is *reduced*. Through modifying the lipid structure we show the dominant determinant of membrane conduction is hydrogen bonds between the phosphate oxygens on adjacent phospholipids. The modulation of conduction with pH is proposed to arise from the varying  $\text{H}_3\text{O}^+$  concentrations altering the molecular area per lipid and modifying the geometry of conductive defects already present in the membrane. Given the geometrical constraints that control the lipid phase structure of membranes, these area changes predict that organisms evolving in environments of different pH will select for different phospholipid chain lengths, such as is found for organisms near highly acidic volcanic vents (short chains) or in highly alkaline salt lakes (long chains). The stabilizing effect of the hydration shells around phosphate groups also accounts for the prevalence of phospholipids across biology. Measurement of ion permeation through lipid bilayers was made tractable using *sparsely* tethered bilayer lipid membranes (tBLMs) with swept frequency electrical impedance spectroscopy (EIS) and ramped DC amperometry. Additional evidence for the effect of pH change on lipid packing density is obtained from neutron reflectometry data of tethered membranes containing perdeuterated lipids.

## INTRODUCTION

In the study of the effects on membrane permeability of both ion channel proteins and peptides it is important to identify all factors that impact the membrane conductivity. The objective of the present study is to characterise one of the major variables determining membrane structure, namely the hydrogen bond strength within and between lipid molecules within the membrane. A key variable in hydrogen bond strength is the pH of the bathing solution. Despite the fact that the concentration of the hydronium ion being three to four orders of magnitude lower than that of others ions (mainly  $\text{Na}^+$  and  $\text{Cl}^-$ ) in the bulk electrolyte solutions, its small size and high electric field gradients can result in it being a dominant factor in membrane integrity. To date, to the best of our knowledge, the impact of pH on membrane conduction remains unreported. In this study we report the dependence of membrane conduction on pH in the range 5 -9 log units. We relate changes in membrane conduction to structural features underlying membrane morphology.

The structures formed by aqueous dispersions of lipids are determined by the balance of forces within the hydrophobic, hydrophilic and interfacial zones of lipid-water aggregates. For a fluid  $\text{L}_\alpha$  lipid lamellar structure this balance of forces has been described in terms of the hydrated molecular area ( $a_o$ ), the lipid leaflet thickness ( $l$ ) and hydrated lipid molecular volume ( $v$ ) <sup>1</sup>. The measure  $v/(a_o l)$  is a qualitative guide to the lipid phases formed by surfactants. The structures formed for  $v/(a_o l) \sim 1$  are lamella bilayers, for  $v/(a_o l) \sim 1/3$  the structures formed are micelles, for  $v/(a_o l) \sim 1/2$  cylindrical tubes, and for  $v/(a_o l) > 1$  a variety of inverted phases <sup>2-3</sup>. In maintaining an appropriate  $v/(a_o l)$  close to unity for lipid bilayers, the area per phospholipid and the resultant membrane thickness will dictate the conformation of all other membrane associated proteins and their physiological functions. This balance is dependent on contributions from both the hydrophobic and hydrophilic components of the membrane and is significantly dependent on the hydration shells surrounding the polar head groups.

The role of hydrogen bonding in determining the balance of forces is evident in all aqueous surfactant assemblies. Increasing the hydrogen ion concentration through lowering the pH is known to cause a decrease in the *critical micelle concentration* (CMC) of sodium dodecyl sulphate (SDS) <sup>4</sup>. Rupert et al (1998) reported significant changes in vesicle fusion and head group clustering for didodecyl phosphate (DDP) vesicles around the effective  $\text{pK}_\text{a}$  of 5.2 <sup>5</sup>. They interpret these effects as arising from protonation of the non-ester phosphate of the DDP. Siegal et al (1989) have also shown that lowering the pH of a DOPE dispersion caused a phase transition from the  $\text{L}_\alpha$  lamellar phase to the Hexagonal II inverted phase ( $\text{H}_{\text{II}}$ ) <sup>6</sup>. This is consistent with a reduction in the area of the hydrated polar group driving the  $\text{L}_\alpha$  phase into the highly curved inverted  $\text{H}_{\text{II}}$  lipid phase.

The major impediment to the passage of ions across lipid membranes is the hydrophobic, low dielectric constant membrane core of the lipid chains. This is a consequence of the high Born energy required to cause an ion to partition into the hydrophobic interior of a lipid bilayer.<sup>7</sup>

That there is a source of the background ionic current despite this high energy cost, has been suggested to arise from sparse and fluctuating “defects” in the bilayer morphology in which hydrophilic pores traverse the non-polar core of the membrane.<sup>8</sup> The incidence of such defects in homogenous fluid phase lipid bilayers will depend on the lipid molecular geometry. The inter-relationship of lipid dimensions,  $v/(a_0 l)$ , indicates that longer chain lipids with smaller areas per molecule will tend to possess fewer pores than short chain lipids with large areas per molecule. This is a consequence of the curvature energy required to form a highly curved toroidal pore traversing the membrane from the inner and to the outer leaflets of the bilayer. The lifetime of toroidal pores is discussed by Karatekin et al (2003).<sup>9</sup> They address the rupture and sealing of liposomes by modelling a balance between the surface pressure arising from intense optical illumination balanced by the line tension of a toroidal pore. The steric contribution, a consequence of the geometrical constraints embodied in  $v/(a_0 l)$ , is termed by these authors as the curvature,  $c_0$ . For planar membranes  $c_0 = 0$ . For membranes possessing positive curvature  $c_0 > 0$  and for negative curvature  $c_0 < 0$ . This term is then added or subtracted from the line tension permitting a calculation of the pore lifetime.

The measurement of ionic permeability through lipid bilayer membranes is experimentally challenging. Patch clamp electrophysiology measures are typically performed on 1  $\mu\text{m}$  diameter membrane patches which, at 1  $M\Omega \text{ cm}^2$  membrane leakage, would require conductance measures to be performed at impedances of greater than  $10^5 \text{ G}\Omega$ , far in excess of the typically measured values of 1 - 10  $\text{G}\Omega$ . This suggests the intrinsic membrane conduction in patch clamp experiments is dominated by mechanisms other than the intrinsic membrane resistance<sup>10</sup>. Solvent-based black lipid membranes (BLMs) suffer not only from high background resistances due to their small areas, but also from the residual solvent in free exchange with the membrane plateau border.<sup>11-12</sup> Further approaches to measuring the intrinsic membrane conduction includes liposomal release assays, which at best, are limited to qualitative measures of conduction due to the uncertainty in the liposome stability. Monolayer techniques performed at the interface between two immiscible electrolyte solutions (ITIES)<sup>13</sup> or measurements employing Langmuir films report on the interfacial properties, but by definition, are unable to describe bilayer permeability or conduction.

The use of electrical impedance spectroscopy (EIS) and ramped direct current amperometry to determine the conduction and capacitance of lipid bilayers provides a unique approach to quantifying ionic permeability. In the present study the conductance of tethered bilayer lipid membranes (tBLMs) is measured in the presence of a range of pH values from 5.0 – 9.0 log units.

In summary we show that decreased pH (increased  $\text{H}_3\text{O}^+$  concentration) reduces the intrinsic membrane conduction by an order of magnitude (pH 9 to pH 5) and significantly decreases water penetration into the membrane. These effects are interpreted as arising from an increase in the hydrogen bond stability caused by neighbouring  $\text{H}_3\text{O}^+$  ions. This interpretation suggests that changes in pH will affect the intrinsic conduction of all phospholipid membranes. Further

data based on neutron reflectometry measures, report on the associated changes in membrane geometry.

## MATERIALS AND METHODS

### *Tethered bilayer lipid membranes*

Using the solvent exchange technique,<sup>14</sup> tBLMs with 10% tethering lipids and 90% spacer lipids (T10 tBLM) were formed. The procedure involves using 2.1 mm<sup>2</sup> pre-prepared tethered benzyl-disulfide (tetra-ethyleneglycol)<sub>n=2</sub> C<sub>20</sub>-phytanyl tethers (DLP) : benzyl-disulfide-tetra-ethyleneglycol-OH spacers in the ratio of 1:9 coated onto 2 mm<sup>2</sup> patterned, 100 nm thick fresh 5N5 gold surfaces sputter coated onto a polycarbonate slide (*SDx Tethered Membranes Pty Ltd, Australia*)<sup>15</sup>. The ratio of tethering molecules to spacer molecules (eg 1:9) is termed here as T10. Similarly, ratios of 1:99 and 0:100 are termed T1 and T100 respectively. Following air drying of this tethered monolayer, 8 µL of a 3 mM solution of a mobile lipid phase dissolved in ethanol is added to a 0.1 mm high, 1µL volume flow cell chamber, and, after a 2 minute incubation, is washed 3 times with 2 x 200 µL of 100 mM NaCl. Mobile lipid phases investigated were: 1-palmitoyl-2-oleoyl-sn-glycero-3-phosphocholine (POPC) (Avanti Lipids, USA); 1,2-dioleoyl-sn-glycero-3-ethylphosphocholine (EPC) (Avanti Lipids USA; 100% diphytanyl-glycero-phosphatidylcholine (DPEPC) (SDx Tethered Membranes Pty Ltd, Australia) (See Fig 2A). As a non-phosphate fully tethered lipid control, tBLMs were prepared employing the fully tethered *membrane spanning lipid terminated with an OH group* (MSLOH) previously described<sup>16</sup> (SDx Tethered Membranes Pty Ltd, Australia). Diagrams of the tethering chemistries are provided in Figure S1 of the Supplementary Material.

The pH of the 100mM NaCl solutions was adjusted by the addition of concentrated HCl or NaOH to create stock solutions of pH ~ 5.0, pH ~ 7.0 and pH ~ 9.0. Each of these solutions was kept in an air-tight container prior to use, and used in within 5 min to minimise any subsequent acidification due to atmospheric CO<sub>2</sub>. The pH of the stock solutions was regularly monitored.

Gramicidin containing membranes were formed as described previously.<sup>15</sup> Briefly, 100 nM of *Gramicidin-A* (BioAustralis Pty Ltd, Australia) was included in the 3mM mobile phase lipid from which the tBLM was formed. Covalently linked bis-gramicidin tBLMs were synthesized as described previously<sup>17</sup>.

*AC impedance spectroscopy* measures were performed using an SDx tethaPod™ operated with SDx tethaQuick™ software (SDx Tethered Membranes Pty Ltd). Swept frequency impedance spectrometry was employed using a 50 mV peak-to-peak AC excitation at 0.1, 0.2, 0.5, 1, 2, 5, 40, 100, 200, 500, and 1000 Hz and zero bias potential. The data were fitted to a *Constant Phase Element* in series with an *Resistor/Capacitor* network<sup>15</sup> using a proprietary adaptation of a Lev Mar fitting routine. This model provided excellent agreement with the data. The use of more complex equivalent circuits<sup>16, 18</sup> to model the defect distribution upon which the

membrane conduction is based was considered to be beyond the scope of the present study. Examples of Bode plots are given in Figure S2 and the equivalent circuit in Figure S3 of the Supplementary Material.

*DC ramped amperometry* measures were performed an eDAQ ER466 Potentiostat.<sup>14</sup> Ramps of 100 V sec<sup>-1</sup> from 0 to 500 mV over 5 ms were applied to T1, T10 and T100 DPEPC tBLMs and to T100 MSLOH tBLMs at pH 5, 7 and 9. The initial current step provides an estimate of the membrane capacitance and the following slope an estimate of the membrane conduction and the onset of additional voltage dependent changes in the membrane conduction.

#### *Neutron Reflectometry (NR) and Data Fitting*

The NR data was collected on the PLATYPUS time-of-flight instrument<sup>19</sup> located at the 20 MW OPAL research reactor (Australian Nuclear Science and Technology Organisation (ANSTO), Sydney, Australia). PLATYPUS is located on a cold neutron guide and as such is supplied with a neutron bandwidth ranging from 2.5 – 18.0 Å with the cut-off being determined by the instrument disc choppers. The Q resolution of the experiment was set at ΔQ/Q of 3.3 % where Q, the scattering vector is defined as

$$Q = (4\pi \sin\theta) / \lambda$$

where θ is the scattering angle and λ is the wavelength of the incident radiation. Incident angles of 0.5, 0.85 and 3.8° were used with the data spliced together after normalisation to the direct beam and background subtraction to produce a single absolutely scaled reflectivity dataset over a Q range of 0.006 to 0.25 Å<sup>-1</sup> using the SLIM reduction package.<sup>20</sup>

Tethered bilayers were formed on 50 mm diameter, 7mm thick, conductive silicon disks that had been coated with chromium then gold at the Melbourne Centre for Nanotechnology. Half membrane spanning T100 tBLMs comprising an inner monolayer of tethered hydrogenated DLP and a perdeuterated DPEPC outer monolayer.<sup>21</sup> Coated disks were clamped to a bespoke perfusion chamber for assembly and measurement at the PLATYPUS sample position.

The hydrogenated and deuterated lipid tails were employed to give neutron contrast between the two leaflets. Further contrast was provided by bathing solutions of 100 mM NaCl in either D<sub>2</sub>O, H<sub>2</sub>O or a HDO mixtures that nominally matched the gold layer. Because of the necessity for measures over extended time periods (~3 hours) the effects arising from dissolved CO<sub>2</sub> causing a drop in pH, 100 mM buffer solutions were employed. For pH 5 acetate buffer was used which was adjusted to the final pH using glacial acetic acid; for pH 7 phosphate buffer was used, and for pH 9 [(cyclohexylamino)ethane sulfonic acid] CHES buffer was used, and both were adjusted to their designated pH value using a NaOH solution. The difference between pH and pD was taken into account when preparing D<sub>2</sub>O-containing buffers and adjusted accordingly so that they were equivalent.

The absolutely scaled data sets were modelled using RasCAL (version 1, A. Hughes, ISIS Spallation Neutron Source, Rutherford Appleton Laboratory) operating within the MATLAB environment. RasCAL uses the standard optical matrix approach of Abeles<sup>22</sup> to calculate the reflectivity. The data modelling was carried out assuming that the interface was composed of a series of parallel layers where the model parameters fitted to the data were scattering length density (SLD), layer thickness and interfacial roughness. Data were simultaneously fitted whereby the structural parameters of the layers were constrained to be equivalent but the SLD allowed to vary with buffer contrast. The SLD for silicon was constrained to  $2.07 \times 10^{-6} \text{ \AA}^{-2}$ . The SLD of the D<sub>2</sub>O buffer solution was fitted based upon the position of the critical edge in the datasets. The final data fits were then assessed via a Markov Chain Monte Carlo resampling method. In this procedure the fitting starting points are randomised and the data fitting repeated 40,000 times. The output from these fits are histogrammed for each parameter with the midpoint taken as the parameter value and the 95% confidence level determined from the distribution.

In order to maximise the observable effects of pH change on the membrane lipid geometry, a fully tethered hydrogenated inner monolayer membrane leaflet and a mobile deuterated outer membrane leaflet was employed. Outer tail thickness and hydration, and headgroup hydration were permitted to vary for a layer model.

## RESULTS

### *Tether density*

**Figures 1A-C** show the effect of pH values of 5, 7 and 9 on the EIS derived conduction values obtained from a phytanyl ether phosphatidyl choline (DPEPC). Tether densities ranged from 1 tether to 99 mobile lipids (1% tethered) to 10 per 90 (10% tethered) to a tBLM in which the inner monolayer was fully tethered and the outer monolayer was mobile (100% tethered). **Figure 1D** shows similar EIS derived conduction data obtained from MSLOH tBLMs, a full membrane spanning non-phosphate containing control. **Figures 1E-H** show current voltage curves (*I-V*) measures on the same samples using DC ramped amperometry. DC ramped amperometry provides a measure of the voltage dependent changes in conduction for each membrane configuration. It is evident that the overall membrane conduction increases with increasing pH in all cases. In addition, as the pH is raised the membrane conduction becomes more sensitive to the voltage ramp. However, with the increase in tethering density both the pH dependence and the voltage dependencies are reduced. In the extreme case of a fully tethered membrane spanning MSLOH, tBLM, the membrane conduction is effectively unaltered by pH or the voltage ramp. In **Figures 1E-H**, the electroporative responses to a 5 ms linear ramp 0 - 500 mV, the initial step reports on the capacitance of the tBLM and the subsequent slope reports on the membrane conduction. A steeper slope reflects a greater conduction. The non-linearity in slope seen at higher voltages<sup>14, 23</sup> reflect an increase in conduction. Smith et al (1984)<sup>24</sup> using free standing lipid bilayers, and later Valincius et al (2008)<sup>25</sup> using sparsely tethered tBLMs, interpret the low activation energy observed for the

intrinsic membrane conduction as ruling out electric field induced channel formation as the mechanism for the induced changes in conduction. Thus, we propose that the non-linear current increases observed here arise, not from the creation of new pores, but from the modulation of existing pores. It is significant that with reduced tethering density the effects of electroporative responses are seen at progressively lower voltages. In particular the voltage dependent background conduction rises steeply as the tether density is lowered below 10% tethers. This is consistent with the dimension required to form a membrane spanning pore between the membrane tethers. These results support the now generally accepted notion that toroidal pores provide the primary mechanism for ionic transport across lipid bilayers.

#### *Lipid class*

The effect of pH on the membrane conduction for bilayers formed from, POPC, DPEPC, EPC and MSLOH is shown in **Figure 2**. The number of potential interfacial hydrogen bonding sites is systematically varied across this family of tBLMs. POPC possesses four types of hydrogen bonding identified in the figure and suffers the largest change (X245) in conduction between pH 5 and pH 9 (**Figure 2C**). DPEPC has the carbonyl sites replaced by the non-hydrogen bonding ethers which results in an intermediate change in conduction (X8.4) between pH 5 and pH 9, and EPC has the non-ester phosphate oxygen-hydrogen bonding site blocked by a ethyl group has a small change in the conduction ratio between pH 5 and pH 9 (X2.9). The MSLOH is a hydroxyl terminated membrane spanning lipid with the potential for only a single hydrogen bond at the outer surface of the tBLM interface with the bulk solvent. This resulted in the smallest change in the conduction ratio between pH 5 and pH 9 (X1.3). Relatively little variation was observed for the membrane capacitance, however, as also seen in **Figure 2C**, the same trend occurs for the change in capacitance as occurred for conduction across the four lipid types.

#### *pH dependence of the reservoir space*

Krishna et al (2003)<sup>16</sup> and Cornell et al (1997)<sup>26</sup> have identified conditions under which the apparent membrane conduction is largely determined by the properties of the reservoir space between the membrane and the supporting electrode. However, as described in Krishna et al (1997), provided *all-ether* chemistries are employed in the fabrication of the tethers these effects are essentially eliminated. In addition, by contrast to these earlier studies, the present report focuses on the pH dependence of membrane conduction rather than the ionic species dependence of membrane conduction. Were the pH dependence of conduction primarily arising from the properties of the reservoir space between the tBLM and the tethering gold electrode, the observed effects would be independent of the presence of an ion channel, or of variations in the lipid class employed to form the tBLM. In **Figure 3** we show the pH dependence of conduction for diphytanyl PC tBLMs with and without a covalently linked dimer analogue of the bacterial ion channel *gramicidin-A*. The concentration of the ion channel employed here is such that the conduction has increased by an amount in excess of two orders of magnitude. As

seen in **Figure 3A**, the pH dependence is less than two-fold when the pH is adjusted from 5 to 9. This is to be compared with the seven-fold change in conduction over the same pH range when employing a diphytanyl PC tBLM (**Figure 3B**), and in excess of a 200-fold change when employing POPC membrane lipids. Furthermore, the reduction of the pH dependence of conduction to less than a two-fold variation over this pH range is consistent with the reported pH dependence of the intrinsic cesium conduction of gramicidin-A channels within diphytanyl PC bilayers.<sup>27</sup> These data argue against a pH dependence of the conduction of the reservoir space as the primary source of conduction variation observed in the current studies. To quantify in detail any residual reservoir effects would require insertion of an ion channel with even smaller pH dependent conductance.

The effect of pH on the conduction of monomeric gramicidin-A channels is shown in **Figure 3C**. Unlike the case of the covalently linked gramicidin dimer, the membrane conduction will now depend upon membrane thickness as has been reported by Mobashery et al (1997).<sup>28</sup> The conduction caused by monomeric *Gramicidin-A* within lipid bilayers arises from the gramicidin monomers aligning within each membrane leaflet to form a conducting dimer.<sup>29</sup> Increasing the H<sub>3</sub>O<sup>+</sup> concentration from pH 9 to pH 5 caused a 2.7 fold decrease in the gramicidin-A induced conduction. The greater pH dependence seen here compared to that for the covalently linked gramicidin dimer (**Figure 3A**) is interpreted as arising from a modulation of the dimer lifetime. The proposed reduction in the area per molecule on reducing the pH from 9 to 5 is further suggested to cause a consequent thickening of the membrane, leading to a reduction in the monomer to dimer on-rate due to a weakening of the hydrogen bonds between the gramicidin-A monomers.<sup>28</sup> In addition, thickening the membrane will increase the dimer to monomer off-rate of the channel. The relatively high concentration of gramicidin-A employed here will minimise these effects, however, it is evident that lowering the pH still induces a significant additional conduction decrease beyond the intrinsic pH dependence of gramicidin conduction.

#### *Neutron Reflectometry*

In order to further explore the effect of pH on the geometry of lipid bilayers, neutron reflectometry measures were acquired using a tBLM comprising a fully hydrogenated inner leaflet and a fully deuterated outer leaflet. These measures were obtained for aqueous bathing solutions comprising various ratios of HDO. The results are presented as the one-dimensional SLD plot for solutions at pH 5, 7 and 9 for three HDO ratios (**Figure 4A**). **Figure 4B** shows the outer tail thickness. As pH is reduced from 9 to 5, the outer leaflet tail thickness is increased by ~4%. Associated with this area thickening of the outer layer leaflet tails is an increase in the lipid volume fraction of 0.95 at pH 5 from 0.89 at pH 9 (**Figure 4C**). In addition, the volume fraction of the outer layer leaflet head groups show an even more dramatic dependence on pH ranging from ~0.87 at pH 5 to ~0.59 at pH 9 (**Figure 4D** and **Table S1** in Supplementary Material). At pH = 9 the outer head group volume fraction was essentially indeterminate.

## DISCUSSION

### *Relative ionic impact of H<sub>3</sub>O<sup>+</sup>*

At pH 5 the 55 M concentration of water and the 100 mM Na<sup>+</sup> concentration greatly exceed the 10 μM H<sub>3</sub>O<sup>+</sup> concentration. However, the biological significance of pH arises from the smaller dimensions of the H<sub>3</sub>O<sup>+</sup> resulting in higher field strengths, and thus more potent non-covalent interactions. Kotyńska and Figaszewski (2005) have reported the electrophoretic measures of monovalent cations across liposomal surfaces of phosphatidylcholine.<sup>30</sup> From these measures they derive the binding density of Na<sup>+</sup> at the membrane surface for a pH range from 0-11. Over the range of pH 6 – 8 they observe a shift in the sodium ion ‘degree of coverage’ from essentially zero to approaching 90%, respectively, indicating a dominant contribution by the H<sub>3</sub>O<sup>+</sup> ions to the Na<sup>+</sup> distribution. These observations are consistent with the results reported here in which the H<sub>3</sub>O<sup>+</sup> concentration also dominates the membrane conduction. The change in the surface Na<sup>+</sup> concentration, as a result of pH changes, may well contribute to morphological changes in the membrane resulting in variations in membrane conduction. Others have proposed, based on molecular dynamics modelling, that the distribution of Na<sup>+</sup> and K<sup>+</sup> at the membrane surface are very different.<sup>31</sup> It is suggested that the Na<sup>+</sup> is located adjacent to the PO<sub>4</sub><sup>−</sup> groups whereas K<sup>+</sup> is excluded from the lipid interface. Our conduction results fail to show any significant difference between Na<sup>+</sup> and K<sup>+</sup> at 100 mM despite a similar pH dependence (data not shown). This suggests that the H<sub>3</sub>O<sup>+</sup> ions have the dominant effect on conduction.

### *Area per lipid*

In the major biological phospholipid families, the fluid L<sub>α</sub> phase area per lipid molecule is in the range of 65 ~75 Å<sup>2</sup>.<sup>32</sup> Lewis and Engelman (1983) report that for lipid chains from C<sub>10</sub> – C<sub>24:1</sub> the area per molecule ( $a_o$ ) was  $68 \pm 2$  Å<sup>2</sup> and the lipid bilayer thickness ( $l$ ) was proportional to acyl chain length.<sup>33</sup> In the crystalline L<sub>β</sub> phase the area per lipid molecule is typically in the range of ~50 Å<sup>2</sup> and dominated by the inter-chain packing.<sup>34</sup> Paresgian et al (1979) have shown, for the fluid phase, that below ~68 Å<sup>2</sup> a significant increase in energy is required to further reduce the hydrated molecular area.<sup>35</sup> Pasenkiewicz-Gierula et al. (1997) report a molecular dynamics simulation of the hydrogen bonding of water to phosphatidylcholine lipids<sup>36</sup>. From their simulation the radial distribution function for the non-ester oxygens bound to the phosphate are within 0.3 % as that for liquid water.<sup>37</sup> Collectively, these reports indicate that the area per lipid in a fluid phospholipid bilayer is dominated by the hydrated lipid headgroup.

### *Hydration shells*

Pasenkiewicz-Gierula et al. (1997) identify the dominant hydrogen bonding pattern for the water populations surrounding the PC headgroup as water molecules directly hydrogen-bonded to the non-ester oxygens of the phosphate group.<sup>38</sup> A further population of associated water molecules, not hydrogen bonded to the lipids, are identified as being consistent with transient

clathrate cages surrounding the choline group. Lopez et al (2004) have extended the Pasenkiewicz-Gierula et al (1997) study and include the extended lifetimes of both the hydrogen bonding and diffusional jumps associated with water in the lipid hydration shells<sup>39</sup>. These molecular dynamic simulations closely correspond to the experimental observations of White and King (1985)<sup>40</sup> who identify a hydration barrier comprising 11-13 water molecules per lipid. One of the few approaches to permit measure of the order of the various populations of water molecules is Sum Frequency Generation Spectroscopy which observes the water order on a time that is short compared to the exchange rate.<sup>41</sup> Using this technique Sovago et al (2009) identify a water population that is isolated from the bulk water and buried between the phosphate and acyl groups of the phospholipid. Collectively, these studies demonstrate the existence of a population of water molecules surrounding the lipid head-groups that is significantly more ordered than bulk water.

#### *Effect of pH on phospholipid area*

The results presented here from EIS, amperometry and neutron reflectometry support a model in which the area per molecule within a lipid assembly is modulated by pH. The primary mechanism for these effects is interpreted in terms of the interaction of the lipid phosphate groups with a hydrating network at the lipid-water interface (**Figure 5**).

Molecular dynamic studies have identified potential hydrogen bonding patterns of water bridging between adjacent phospholipid molecules via the non-ester oxygens of the lipid phosphate groups.<sup>36,38</sup> Further hydrogen bonded bridging water molecules are proposed to exist between the non-ester phosphate oxygens and the carbonyl oxygens in esterified phospholipids. In the present study it is shown that substantial changes in conduction occur over the two to four orders of magnitude change in the H<sub>3</sub>O<sup>+</sup> concentration, with the conduction being reduced at the highest H<sub>3</sub>O<sup>+</sup> concentrations (low pH) across all phospholipid species studied here. It is proposed that the H<sub>3</sub>O<sup>+</sup> ions compete with and disrupt the hydrogen bonding pattern of the intermolecular bridging water molecules causing the observed variation in membrane conductivity, primarily through variations in the molecular area. A further insight by molecular dynamics is the contribution made by bridging water molecules for an ether or ester linked phospholipid.<sup>36, 38</sup> **Figure 2A** shows a mechanism whereby the hydrogen bonds between individual water molecules and their neighbouring phospholipid phosphate or carbonyl oxygens can be disrupted by a less anisotropic H<sub>3</sub>O<sup>+</sup> ion causing a disruption in the bridging hydrogen bonds and a condensation of the phospholipid onto the positively charged H<sub>3</sub>O<sup>+</sup> resulting in a reduction in the area occupied per phospholipid. In addition, the conduction at pH ~ 5 in sparsely 10% tethered tBLMs comprising 100% EPC or 100% DPEPC or 100% POPC is shown in **Figure 2B**. The conduction is found to progressively increase in the order of POPC < DPEPC < EPC. In the case of POPC it is proposed that the conduction is the smallest due to the attraction of the H<sub>3</sub>O<sup>+</sup> ions to both carbonyl and non-ester phosphate oxygens. The ~ 2-fold higher conduction seen in DPEPC is proposed to be as a result of the elimination of the negative carbonyl oxygen creating a smaller reduction in the molecular area. The ~ 5-fold

higher conduction seen in EPC is proposed to arise from the blocking effects of the non-ester phosphate oxygen bound ethyl group both reducing the attractive charge and sterically impeding the area reduction.

Further consequences of this model are demonstrated in **Figure 2B** where the conduction at pH ~ 9 is shown for the same family of lipids. At this high pH the POPC the carbonyl and oxygen sites would thus be surrounded by un-dissociated water resulting in the largest molecular area and therefore highest conductivity. The lower conductances seen for EPC and DPEPC would arise from the hydrophobic and steric blocking caused by the non-ester phosphate oxygen ethyl group for the EPC, and the absence of the ester carbonyls for the DPEPC.

#### *Membrane Thickness and pH*

The effect of pH on tBLM thickness was further investigated by including the ion channel gramicidin-A<sup>28</sup>. It can be seen in **Figure 3C** that lowering the pH caused a decrease in conduction consistent with a thicker membrane causing a reduction in the gramicidin-A dimer lifetime. It should be noted, the similar reduction seen for the same tBLM in the absence of gramicidin-A also arises from a reduction in the molecular area, however, we propose these effects in the absence of gramicidin-A arise from the modulation of the toroidal pore defect diameter driven by changes in the molecular geometry of the lipid. These observations are supported by a direct measure of the contraction of the area of a monolayer of phospholipid on a Langmuir trough as reported by Gong et al (2002).<sup>42</sup> Measurements of variations in membrane thickness based on capacitance observations are complicated by uncertainties of the interfacial dielectric constant for the different values of pH. Other contributions to the pH dependence of the gramicidin-A conduction may arise from a small modulation of the diffusion coefficient of both the lipid and gramicidin-A impacting the monomer to dimer on-rate.

From the neutron reflectometry results additional evidence is available on the pH dependence of the outer bilayer lipid leaflet. It was observed that over the pH range from 5 – 9 log units the outer bilayer leaflet thickness decreased by ~3 – 4 %. This is an indication that the molecular area has increased over this pH range by ~6 – 8 %. These changes in molecular geometry will be reflected in changes in the geometry of membrane spanning defects described here as toroidal pores. Increasing the intrinsic molecular area across the tBLM drives an increase in the average pore diameter, causing an increase in conduction.

#### *The Modulation of Toroidal Pores by pH*

The tBLM conduction is modelled here as arising from the modulation of fluctuating toroidal pores that are *already* present within the membrane and traverse the otherwise essentially ion impermeable hydrocarbon core of the lipid bilayer. That the conduction variation arises from existing toroidal pores rather than the creation of new pores is demonstrated by the approximately 35-38 kJ/mol activation energy for the intrinsic bilayer conduction.<sup>24-25</sup> This low

value of activation energy for conduction eliminates other explanations requiring the creation of new pores for which activation energies in excess of 100 kJ/mol are required.<sup>24, 43</sup>

Increasing the pH results in both an increase in the molecular area per hydrated molecule and in the intrinsic membrane conduction. We assign the conduction increase to the primary effect of pH increasing the local hydrated molecular area resulting in a re-distribution of the membrane lipids between the bilayer regions and the toroidal pores favouring greater numbers within toroidal pore defects already within the membrane. This causes the average diameter and conduction of these defects to increase. The origin of the increase in diameter of the toroidal pores is a result of relaxing the *critical packing parameter* (CPP), or  $v/(a_0l)$ , to nearer unity as the pH drives an increase in hydrated molecular area. Within the toroidal pore the CPP is between 1/2 and 1/3. With the increased hydrated molecular area driving the CPP away from the bilayer geometry a lateral pressure is introduced that is relaxed by the lipids diffusing into the curved regions of the pore. With the increased area caused by the increased pH, an increase in the pore diameter occurs, permitting more membrane lipids to be accommodated within the highly curved low CPP region, with the associated effect of causing an increase in the membrane conduction (**Figure 6**). This effect will relax the geometrical constraints on the overall membrane until the lateral redistribution of membrane lipid causes the pore diameter to approach the bilayer thickness at which point the process is no longer reversible and the membrane conduction irreversibly increases. This effect was evident following excursions to pH values exceeding 9 log units (data not shown).

## CONCLUSIONS

A clear conclusion from this study is the significant decrease in membrane conduction at low pH across all phospholipid types. In the absence of a phosphate group there was no significant change in conduction with the same changes in pH. We propose the role of the phosphate in membrane geometry and stability arises from the hydration shells associated with the phosphate groups being commensurate with the hydrogen bonding geometry of water molecules. The area decrease according to this model primarily arises from the progressively greater attractive force between the phosphate and carbonyl oxygens mediated by the different charged states of water. The introduction of  $\text{H}_3\text{O}^+$  ions sequestered to the region of the negatively charged phosphate oxygens strengthens the hydrogen bonding network, reducing the hydrated molecular area, increasing membrane thickness, and reducing the ionic conduction. In this model the observed decrease in membrane conduction is proposed to arise from a decrease in the average toroidal pore diameter due to a redistribution of lipids between the highly curved region within the toroidal pores (CPP 1/2 - 1/3) and the planar regions (CPP ~ 1) of the bilayer. This supports the proposition that an important factor in the evolution of stable biological membranes across plants, bacteria and animals has been the occurrence of a phosphate group within the primordial surfactant population. It could be significant that bacteria found in highly alkaline salt lakes possess longer chained lipids<sup>44</sup>. This may be in order to sustain the geometrical constraint of the CPP close to unity to permit the formation of

lamellar structures at high pH. Similarly, some extremophile bacteria found adjacent to volcanic vents may possess short chain lipids<sup>45</sup> to accommodate the same geometrical constraint for the very low pH conditions resulting from vented sulphur dioxide. In conclusion, the ubiquity of phospholipid bilayers in biology poses the question of the evolutionary advantage of a phosphate group and its hydration shell within the composition of lipidic biomembranes. As the present study suggests, this phosphate hydration shell plays an important role in determining the membrane structure, stability and conductivity.

## ACKNOWLEDGEMENTS

We wish to thank Dr Paul Duckworth for valuable discussions concerning this work. Experiments were undertaken by TB, CGC, HA, KRH, and SC. Neutron Reflectometry experiments were undertaken by TB, CGC, SAH and APLB with data fitting by SAH. Experiments were designed by CGC, BC, SAH. HC and SV assisted with theoretical discussions. Manuscript was written by CGC and BC and subsequently edited by all authors. This work was supported by the *Australia Research Council Linkage Program* (LP120200078) Discovery Program (DP160101664). APLB is supported by an Australian Research Council Development Early Career Researcher Award (DE140101788). Access to the PLATYPUS Neutron Reflectometer was supported by the *Australian Nuclear Science and Technology Organisation* (ANSTO) beam proposals P4473 and P4469. BC is a shareholder, and SC an employer, of SDx Tethered Membranes Pty Ltd.

## SUPPORTING INFORMATION AVAILABLE

Supplementary material for this work provides diagrams of the tethering chemistries used for the creation of tBLMs used in this study (Figure S1); sample Bode plots of tBLMs at pH 5, 7 and 9 (Figure S2) fitted to an equivalent circuit (Figure S3); a Table detailing the 95% confidence intervals for the neutron scattering fits (Table S1); and an inset with expanded scale of Figure 4A, which is a plot of scattering length density versus distance at different pH values with varying contrasts (Figure S4). This information is available free of charge via the Internet at <http://pubs.acs.org/>.

## REFERENCES

1. Israelachvili, J. N.; Mitchell, D. J.; Ninham, B. W., Theory of self-assembly of hydrocarbon amphiphiles into micelles and bilayers. *J. Chem. Soc., Faraday Trans. 2* **1976**, 72, 1525-1568.
2. Wennerström, H.; Lindman, B., Micelles. Physical chemistry of surfactant association. *Phys. Rep.* **1979**, 52 (1), 1-86.
3. Israelachvili, J.; Marçelja, S.; Horn, R. G., Physical principles of membrane organization. *Quarterly reviews of biophysics* **1980**, 13 (02), 121-200.
4. Rahman, A.; Brown, C., Effect of pH on the critical micelle concentration of sodium dodecyl sulphate. *J. Appl. Polym. Sci* **1983**, 28 (4), 1331-1334.
5. Rupert, L. A. M.; Van Breemen, J. F. L.; Hoekstra, D.; Engberts, J. B. F. N., pH-dependent fusion of didodecyl phosphate vesicles: role of hydrogen-bond formation and membrane fluidity. *J. Phys. Chem.* **1988**, 92 (15), 4416-4420.

6. Siegel, D.; Burns, J.; Chestnut, M.; Talmon, Y., Intermediates in membrane fusion and bilayer/nonbilayer phase transitions imaged by time-resolved cryo-transmission electron microscopy. *Biophys. J.* **1989**, *56* (1), 161.
7. Parsegian, A., Energy of an ion crossing a low dielectric membrane: solutions to four relevant electrostatic problems. *Nature* **1969**, *221* (5183), 844-846.
8. Bennett, W. F. D.; Sapay, N.; Tieleman, D. P., Atomistic Simulations of Pore Formation and Closure in Lipid Bilayers. *Biophys. J.* **2014**, *106* (1), 210-219.
9. Karatekin, E.; Sandre, O.; Guitouni, H.; Borghi, N.; Puech, P.-H.; Brochard-Wyart, F., Cascades of Transient Pores in Giant Vesicles: Line Tension and Transport. *Biophys. J.* **2003**, *84* (3), 1734-1749.
10. Hamill, O. P.; Marty, A.; Neher, E.; Sakmann, B.; Sigworth, F., Improved patch-clamp techniques for high-resolution current recording from cells and cell-free membrane patches. *Pflügers Archiv* **1981**, *391* (2), 85-100.
11. Ashcroft, R.; Coster, H.; Smith, J., The molecular organisation of bimolecular lipid membranes. The dielectric structure of the hydrophilic/hydrophobic interface. *Biochim. Biophys. Acta, Biomembr.* **1981**, *643* (1), 191-204.
12. Naumowicz, M.; Figaszewski, Z. A.; Poltorak, L., Electrochemical impedance spectroscopy as a useful method for examination of the acid-base equilibria at interface separating electrolyte solution and phosphatidylcholine bilayer. *Electrochim. Acta* **2013**, *91*, 367-372.
13. Arrigan, D. W., Bioanalytical detection based on electrochemistry at interfaces between immiscible liquids. *Anal. Lett.* **2008**, *41* (18), 3233-3252.
14. Cranfield, Charles G.; Cornell, Bruce A.; Grage, Stephan L.; Duckworth, P.; Carne, S.; Ulrich, Anne S.; Martinac, B., Transient Potential Gradients and Impedance Measures of Tethered Bilayer Lipid Membranes: Pore-Forming Peptide Insertion and the Effect of Electroporation. *Biophys. J.* **2014**, *106*, 182-189.
15. Cranfield, C. G.; Bettler, T.; Cornell, B., Nanoscale Ion Sequestration To Determine the Polarity Selectivity of Ion Conductance in Carriers and Channels. *Langmuir* **2015**, *31*, 292-298.
16. Krishna, G.; Schulte, J.; Cornell, B. A.; Pace, R. J.; Osman, P. D., Tethered Bilayer Membranes Containing Ionic Reservoirs: Selectivity and Conductance. *Langmuir* **2003**, *19* (6), 2294-2305.
17. Prashar, J.; Sharp, P.; Scarffe, M.; Cornell, B., Making lipid membranes even tougher. *J. Mater. Res.* **2007**, *22* (08), 2189-2194.
18. Valincius, G.; Meškauskas, T.; Ivanauskas, F., Electrochemical impedance spectroscopy of tethered bilayer membranes. *Langmuir* **2012**, *28*, 977-90.
19. James, M.; Nelson, A.; Holt, S.; Saerbeck, T.; Hamilton, W.; Klose, F., The multipurpose time-of-flight neutron reflectometer “Platypus” at Australia’s OPAL reactor. *Nucl. Instrum. Methods Phys. Res., Sect. A* **2011**, *632* (1), 112-123.
20. Nelson, A. In *Motofit—integrating neutron reflectometry acquisition, reduction and analysis into one, easy to use, package*, J. Phys.: Conf. Ser., IOP Publishing: 2010; p 012094.
21. Yepuri, N. R.; Holt, S. A.; Moraes, G.; Holden, P. J.; Hossain, K. R.; Valenzuela, S. M.; James, M.; Darwish, T. A., Stereoselective synthesis of perdeuterated phytanic acid, its phospholipid derivatives and their formation into lipid model membranes for neutron reflectivity studies. *Chem. Phys. Lipids* **2014**, *183*, 22-33.
22. Abelès, F., La théorie générale des couches minces. *J. Phys. Radium* **1950**, *11* (7), 307-309.
23. Hoiles, W.; Krishnamurthy, V.; Cranfield, C. G.; Cornell, B., An engineered membrane to measure electroporation: effect of tethers and bioelectronic interface. *Biophys. J.* **2014**, *107*, 1339-51.
24. Smith, J.; Laver, D.; Coster, H., The conductance of lecithin bilayers: The dependence upon temperature. *Chem. Phys. Lipids* **1984**, *34* (3), 227-236.
25. Valincius, G.; Heinrich, F.; Budvytyte, R.; Vanderah, D. J.; McGillivray, D. J.; Sokolov, Y.; Hall, J. E.; Lösche, M., Soluble amyloid  $\beta$ -oligomers affect dielectric membrane properties by bilayer insertion and domain formation: implications for cell toxicity. *Biophys. J.* **2008**, *95* (10), 4845-4861.

26. Cornell, B. a.; Braach-Maksvytis, V. L.; King, L. G.; Osman, P. D.; Raguse, B.; Wieczorek, L.; Pace, R. J., A biosensor that uses ion-channel switches. *Nature* **1997**, *387*, 580-583.
27. Rostovtseva, T. K.; Aguilella, V. M.; Vodyanoy, I.; Bezrukov, S. M.; Parsegian, V. A., Membrane surface-charge titration probed by gramicidin A channel conductance. *Biophys. J.* **1998**, *75* (4), 1783-1792.
28. Mobashery, N.; Nielsen, C.; Andersen, O. S., The conformational preference of gramicidin channels is a function of lipid bilayer thickness. *FEBS Lett.* **1997**, *412* (1), 15-20.
29. Wallace, B. A.; Veatch, W. R.; Blout, E. R., Conformation of gramicidin A in phospholipid vesicles: circular dichroism studies of effects of ion binding, chemical modification, and lipid structure. *Biochemistry* **1981**, *20* (20), 5754-5760.
30. Kotyńska, J.; Figaszewski, Z., Adsorption equilibria between liposome membrane formed of phosphatidylcholine and aqueous sodium chloride solution as a function of pH. *Biochim. Biophys. Acta, Biomembr.* **2005**, *1720* (1), 22-27.
31. Vácha, R.; Siu, S. W.; Petrov, M.; Böckmann, R. A.; Barucha-Kraszewska, J.; Jurkiewicz, P.; Hof, M.; Berkowitz, M. L.; Jungwirth, P., Effects of Alkali Cations and Halide Anions on the DOPC Lipid Membrane†. *J. Phys. Chem. A* **2009**, *113* (26), 7235-7243.
32. Luzzati, V.; Husson, F., The structure of the liquid-crystalline phases of lipid-water systems. *J. Cell Biol.* **1962**, *12* (2), 207-219.
33. Lewis, B. A.; Engelman, D. M., Lipid bilayer thickness varies linearly with acyl chain length in fluid phosphatidylcholine vesicles. *J. Mol. Biol.* **1983**, *166* (2), 211-217.
34. Sun, W.-J.; Suter, R.; Knewton, M.; Worthington, C.; Tristram-Nagle, S.; Zhang, R.; Nagle, J., Order and disorder in fully hydrated unoriented bilayers of gel-phase dipalmitoylphosphatidylcholine. *Phys. Rev. E* **1994**, *49* (5), 4665.
35. Parsegian, V. a.; Fuller, N.; Rand, R. P., Measured work of deformation and repulsion of lecithin bilayers. *Proc. Natl. Acad. Sci.* **1979**, *76*, 2750-2754.
36. Pasenkiewicz-gierula, M.; Takaoka, Y.; Miyagawa, H.; Kitamura, K., Hydrogen Bonding of Water to Phosphatidylcholine in the Membrane As Studied by a Molecular Dynamics Simulation : Location , Geometry , and Lipid - Lipid Bridging via Hydrogen-Bonded Water. *J. Phys. Chem. A* **1997**, *5639*, 3677-3691.
37. Soper, A. K., The radial distribution functions of water and ice from 229 to 673 {K} and at pressures up to 400 {MPa}. *Chem. Phys.* **2000**, *258*, 121-137.
38. Pasenkiewicz-Gierula, M.; Takaoka, Y.; Miyagawa, H.; Kitamura, K.; Kusumi, A., Charge pairing of headgroups in phosphatidylcholine membranes: a molecular dynamics simulation study. *Biophys. J.* **1999**, *76* (3), 1228-1240.
39. Lopez, C. F.; Nielsen, S. O.; Klein, M. L.; Moore, P. B., Hydrogen bonding structure and dynamics of water at the dimyristoylphosphatidylcholine lipid bilayer surface from a molecular dynamics simulation. *J. Phys. Chem. B* **2004**, *108* (21), 6603-6610.
40. White, S. H.; King, G. I., Molecular packing and area compressibility of lipid bilayers. *Proc. Natl. Acad. Sci.* **1985**, *82* (19), 6532-6536.
41. Sovago, M.; Vartiainen, E.; Bonn, M., Observation of buried water molecules in phospholipid membranes by surface sum-frequency generation spectroscopy. *J. Chem. Phys.* **2009**, *131* (16), 161107.
42. Gong, K.; Feng, S.-S.; Go, M. L.; Soew, P. H., Effects of pH on the stability and compressibility of DPPC/cholesterol monolayers at the air–water interface. *Colloids Surf., A* **2002**, *207* (1), 113-125.
43. Coster, H., The physics of cell membranes. *J. Biol. Phys.* **2003**, *29* (4), 363-399.
44. de Rosa, M.; Gambacorta, a.; Nicolaus, B.; Grant, W. D., A C25,C25 Diether Core Lipid from Archaeabacterial Haloalkaliphiles. *Microbiology* **1983**, *129*, 2333-2337.
45. Mykytczuk, N.; Trevors, J.; Ferroni, G.; Leduc, L., Cytoplasmic membrane fluidity and fatty acid composition of Acidithiobacillus ferrooxidans in response to pH stress. *Extremophiles* **2010**, *14* (5), 427-441.



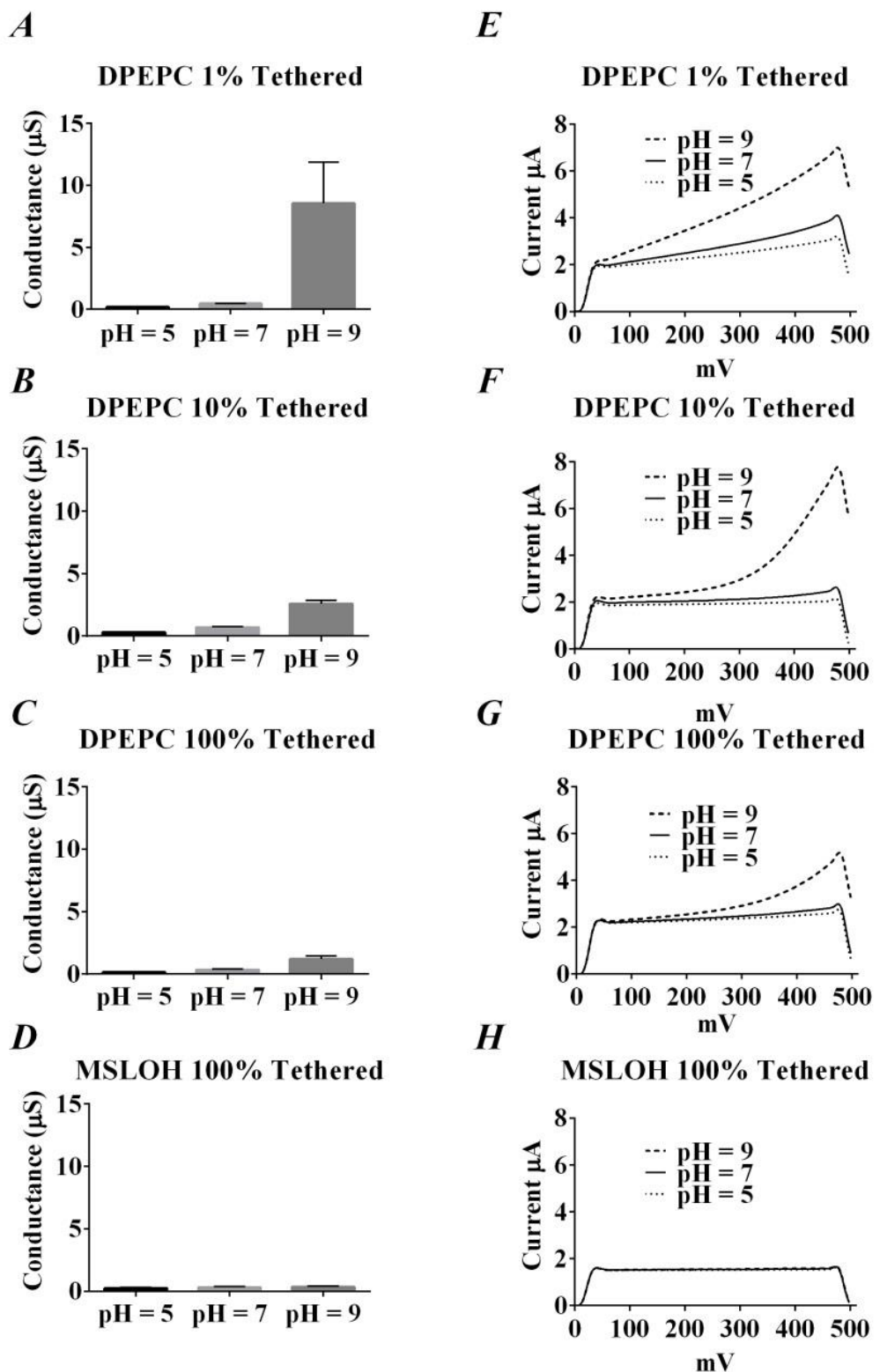
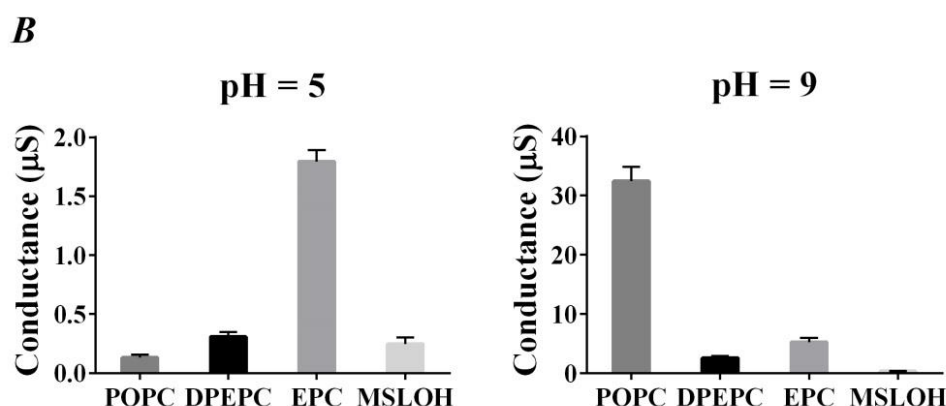
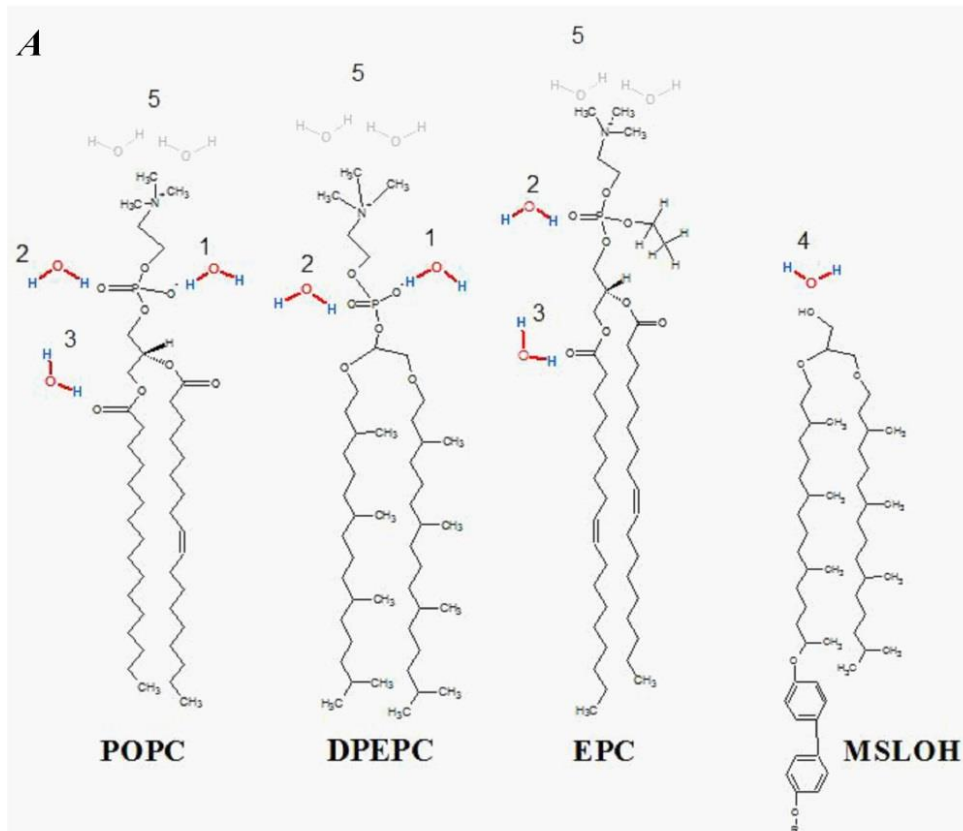


**Figure 1 A-D**, conductance ( $\mu\text{S}$ ) at pH 5, 7, and 9. **A**, 1% mol:mol tethers:spacers (n=4); **B**, 10% mol:mol tethers:spacers (n=6); **C**, 100% tethers anchoring a mobile DPEPC lipid

bilayer (n=5). In C, the DPEPC forms a monolayer over the fully tethered inner leaflet. **D**, 100% MSLOH fully membrane spanning tBLM (n=5). **E-H**, select examples of ramped amperometry spectra of the same membrane architectures at pH 5, 7 and 9. All measures taken at room temperature of 20-22°C.



**C**

	POPC	DPEPC	EPC	MSLOH
Ratio pH 9:pH 5 Conductance	245	8.4	2.9	1.3
Ratio pH 9:pH 5 Capacitance	1.12	1.08	1.07	1

**Figure 2. A** POPC, DPEPC, EPC and MSLOH molecules in which 4 hydrogen bonding sites are identified: at 1) the *non-ester phosphate oxygen*, at 2) the *ester phosphate oxygen* at 3) the *carbonyl oxygens* and at 4) the hydroxyl group of the MSLOH; all of which may hydrogen bond cross-link through water to similar sites on adjacent phospholipids. At 5) a further population is identified with a weakly hydrogen-bonded *clathrate hydration shell* surrounding

the choline group. **B**, conductance ( $\mu\text{S}$ ) for each lipid POPC (n=4), DPEPC (n=6), EPC (n=3) as 10% tethered tBLMs and 100% tethered MSLOH (n=5), at pH 5 and at pH 9 (*N.B. the scale difference*). **C**, table shows the ratios of both conduction and capacitance between pH 5 and pH 9 for the three lipids and MSLOH.

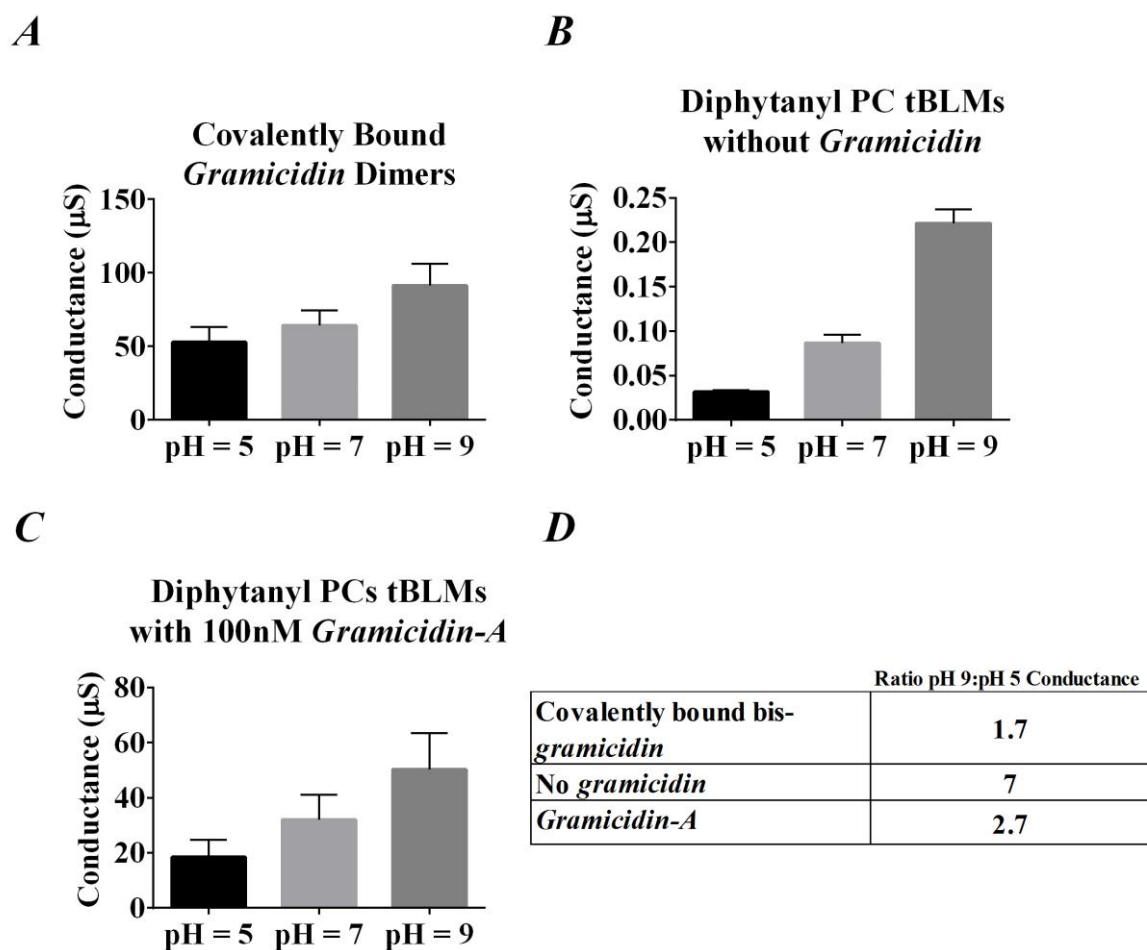


**Figure 3** **A**, mean conduction in a fully tethered membrane spanning tBLM containing covalently linked bis-gramicidin (n=3). **B**, mean conduction in an equivalent membrane without gramicidin (*N.B. the scale difference*) (n=5). **C**, mean conduction ( $\mu\text{S}$ ) of 10% tethered diphytanyl PC tBLMs containing 100 nM gramicidin-A at pH 5, 7 and 9 (n=5). **D**, table shows the ratios of conduction between pH 5 and pH 9 for the three cases depicted in **A**, **B**, **C**.

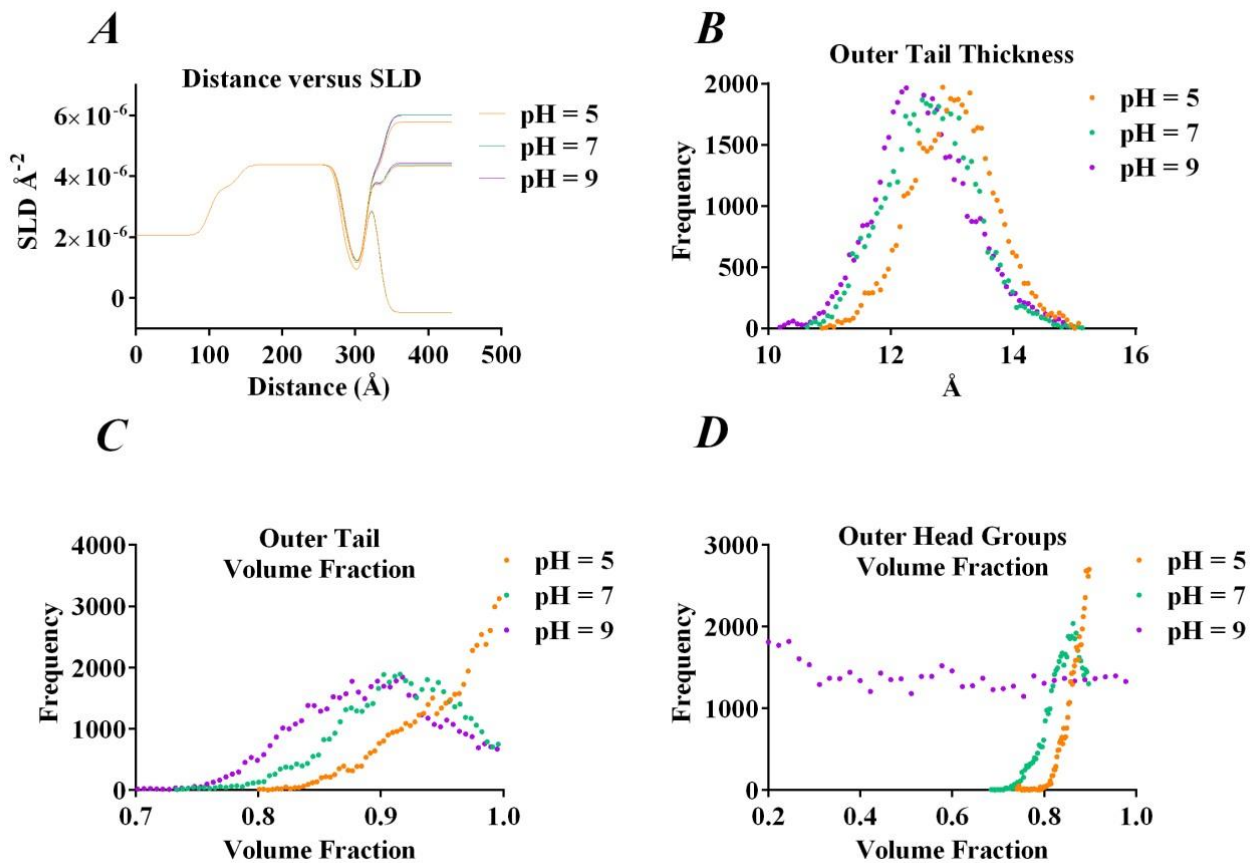


**Figure 4 A,** Distance versus SLD plots at pH values of 5, 7 and 9 for three contrasts of  $\text{H}_2\text{O}$ ,  $\text{D}_2\text{O}$  and a gold matched mixture of  $\text{H}_2\text{O}$  (25%) and  $\text{D}_2\text{O}$  (75%). An enlarged version of this figure from  $250 \text{ \AA} - 500 \text{ \AA}$  is provided as S4 in Supplementary Material. **B**, histogram of 40,000 modelled fits of the outer deuterated lipid leaflet tail thickness at pH 5, 7 and 9. **C**, histogram of 40,000 modelled fits of the outer deuterated lipid leaflet tails volume fraction at pH 5, 7 and 9. **D**, histogram of 40,000 modelled fits of the outer deuterated lipid leaflet head group volume fraction at pH 5, 7 and 9.

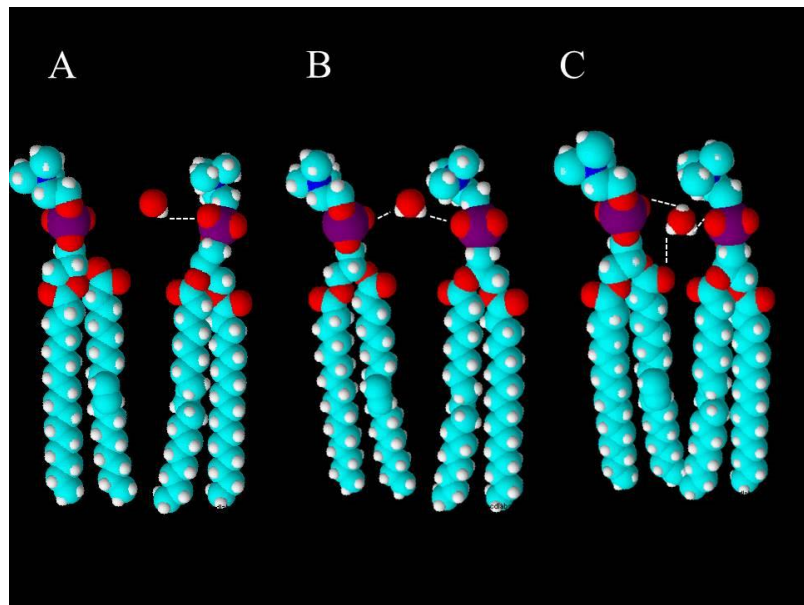


**Figure 5**, Schematic of phosphatidyl choline hydrogen bonded through the phosphate and carbonyl oxygens of adjacent lipids through water intermediaries. **A**, at high pH the charged intermediary being a hydroxyl molecule ( $\text{OH}^-$ ). **B**, at neutral pH the prevalent intermediary being a water molecule ( $\text{H}_2\text{O}$ ). **C**, at low pH the charged intermediary being an hydronium ion ( $\text{H}_3\text{O}^+$ ).

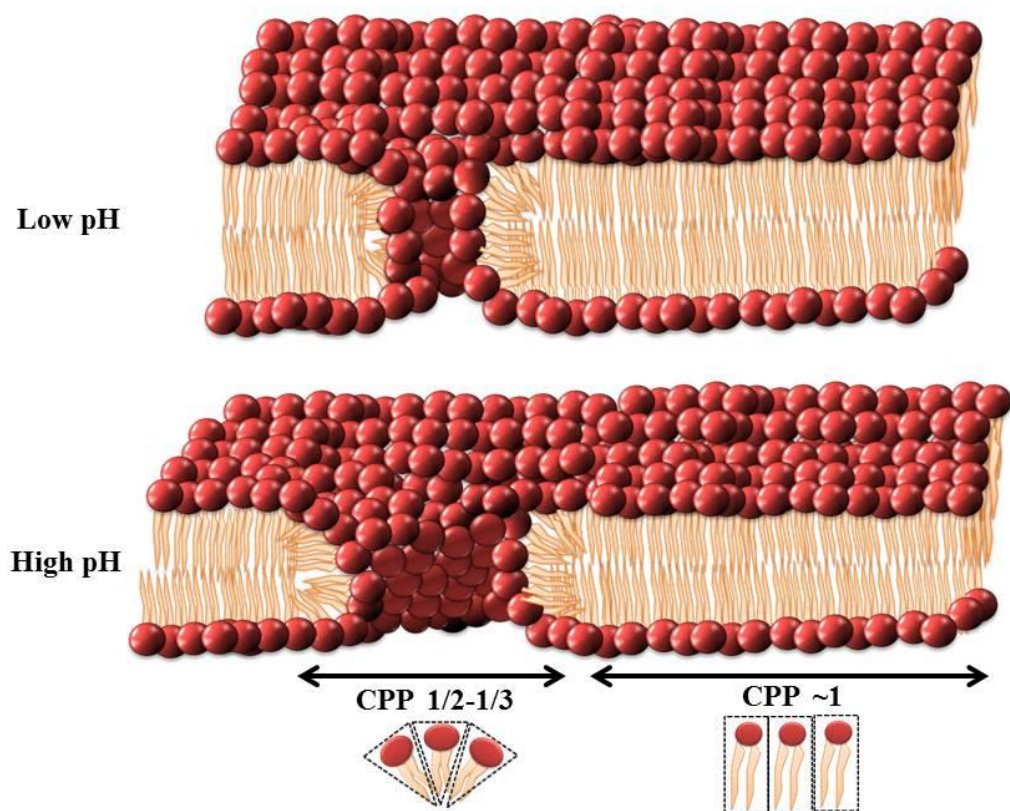


**Figure 6**, Schematic of proposed toroidal pore variations due to pH. In order to accommodate a decrease in the CPP at high pH more lipids diffuse into the curved regions of toroidal pores increasing their surface area and making the bilayer more conductive to ions.

## TOC Graphic

